Copyright © 1998, by the International Council of the Aeronautical Sciences (ICAS)
and the American Institute of Aeronautics and Astronautics, Inc.

ICAS-98-3,3,3

A98-31541

IN-FLIGHT SHOCK DETECTION USING HOT FILM SENSORS AND CONSTANT VOLTAGE ANEMOMETER SYSTEM

S. M. Mangalam, G. R. Sarma
Tao Systems, Inc.
Williamsburg, Virginia

T. R. Moes
NASA Dryden Flight Research Center
Edwards, California

Abstract

Transonic shock locations were successfully detected in flight tests conducted at NASA Dryden Flight Research Center on a F-15B aircraft using a 10"-chord modified NACA 0021 airfoil instrumented with hot-film sensors. The hot-film sensors were operated by a bank of automated constant voltage anemometer system installed in the Flight Test Fixture (FTF). The airfoil was designed to generate transonic shocks at speeds above Mach 0.7. Shock location estimated by in-flight pressure measurements were used to correlate the hot-film measurements. Hot-film measurements were also used to determine the state of the boundary layer (laminar, transitional, or turbulent).

Introduction

Transonic shock and its interactions with boundary layer have significant impact on the performance and safety of high-speed flight vehicles. Simulation of transonic aerodynamic characteristics using wind tunnel models is associated with numerous problems because of the very complex nature of the flow. Important aircraft safety-related characteristics such as buffet and transonic flutter are critically dependent on the state of the boundary layer at the shock location. Difficulties encountered in correctly simulating the full-scale transonic shock characteristics in wind tunnels have led to significant errors in predicting aircraft transonic performance and handling qualities[1]. Consequently, measurements of transonic shock locations on a full-scale aircraft is desired to correlate results with computational fluid dynamics (CFD) and wind-tunnel predictions.

Transonic shock and its interactions with boundary layers have been investigated by many authors[e.g., 2-5]. Typically the adverse pressure gradient induced by the shock would cause local separation of the boundary-layer flow. A hypothetical structure of the shock-boundary-layer interaction region is shown in Fig. 1. One of the important effects of the shock in transonic flows is the presence of flow separation at the foot of the lambda-shock. The extent and the subsequent behavior of the shock-induced separated flow region is dictated by the shock strength, among other flow characteristics, such as the state of the boundary layer at the shock location, and has severe impact on the vehicle performance and safety.

Traditionally optical techniques and pressure measurements have been used to estimate shock location by post-processing of the data. Real-time identification of shock location with pressure measurements is difficult because of the severe dynamic response limitations. Surface hot-film sensors are considered a potential alternative to pressure measurements for shock location sensing for several reasons. These reasons include easier installation and operation, higher frequency response, and better spatial resolution, as in many cases hot-film sensors can be placed close together. Hot films also provide information on the location and dynamics of critical boundary-layer flow features such as the laminar-to-turbulent transition, flow separation and reattachment regions[6-9]. Once calibrated, the same sensors can also provide surface skin-friction distribution[10-16]. The present paper describes some results from flight tests conducted to demonstrate the effectiveness and the potential of constant voltage hot-film anemometer technology for the flight R&D studies of transonic aerodynamics.

Successful flight tests were conducted using the NASA Dryden Flight Research Center's F-15B Flight Test Fixture (FTF) to detect transonic shock on a modified NACA0021[17] airfoil section instrumented with an array of micro-thin, multi-element surface hot-film sensors.

Copyright © 1998 by ICAS and AIAA. All rights reserved

Copyright © 1998, by the International Council of the Aeronautical Sciences (ICAS)
and the American Institute of Aeronautics and Astronautics, Inc.

These hot films were operated by an automated 16-channel constant voltage anemometer instrumentation system. The airfoil model was also instrumented with upper surface pressure orifices. The hot-film outputs were correlated to the shock location estimates inferred from the pressure measurements. Both laminar and tripped boundary layers were investigated. Flight tests were conducted at an altitude of 20,000 ft and Mach numbers 0.68 through 0.8. Tests were conducted under stabilized alpha as well as under variable alpha and Mach number conditions. Some results from these flight tests along with details of the FTF and instrumentation system were reported earlier[18].

Flight Experiments

Flight Test Fixture (FTF)

Installed on the lower fuselage centerline of the NASA F-15B aircraft (Fig. 2), the FTF uses the same hardware attachment points as the standard centerline fuel tank. The FTF was created as a test-bed for generic aerodynamics research [19] and is 107 in. long, 32 in. high, and 8 in. wide with a 12° elliptical nose section and blunt trailing edge. A noseboom is mounted at the leading edge of the FTF to measure Pitot and static pressures and local flow angles.

For this experiment, a total temperature probe was installed on the left side of the FTF near the trailing edge. The test article for this experiment was mounted[18] on the left side of the FTF, approximately 87 in. aft of the leading edge and 9.6 in. from the bottom. Data were telemetered to a ground control room for real-time monitoring and recording.

Test Article

The aluminum test article consisted of a low-aspect-ratio wing with a modified NACA 0021 airfoil section. The unswept wing had an 8.5 in. span and a 10 in. chord. The lower airfoil surface was flattened and the trailing edge was blunted to allow internal installation of pressure ports and the routing of electrical leads from the surface-mounted hot films. Sixty-two flush pressure ports were installed on the upper surface as shown in Fig. 3.

Stainless steel tubing with internal diameter of 0.031 in. was used to plumb the pressure ports. The pressure tubing was routed into the FTF and connected to flexible tubing (0.055 in. internal diameter) once inside the FTF. A polyimide sheet containing the hot films and associated wire leads covered the entire upper surface of the airfoil. Pressure port holes were drilled through this sheet.

The actual hot-film sensors were placed at the same chord locations as the pressures (Fig. 3). The electrical leads from the hot-film sensors were routed along the top of the test article outward and forward and then around the leading edge (Fig. 3) and through a slot in the lower surface into the test article. The leads were then directed into the FTF and connected to the CVA circuits.

Instrumentation

Air Data

The FTF pitot-static measurements were corrected for position error to obtain freestream measurements of Mach, ambient pressure, and dynamic pressure. The FTF total temperature probe was used with Mach number to obtain freestream ambient temperature. An angle-of-attack vane was also installed on the FTF noseboom to provide local angle-of-attack forward of the FTF but the angle of attack at the test article was appreciably different from that forward of the FTF because of fuselage flow straightening[19]. Consequently, no direct measurements of local angle of attack were made at the test article. All air data parameters were measured and recorded at 52 Hz.

Pressure Measurements

Pressure measurements from the upper surface were obtained using two 32-port electronically scanned pressure transducer modules. These modules measured the difference between the surface pressure and a reference pressure. The reference pressure was from the static pressure source on the FTF noseboom and measured using a 0-19 psia 20-bit digital pressure transducer. The forward port pressures were measured with a ±10 psid module, and the aft pressure ports were measured with a ±5 psid module. Approximately 3 ft of pressure tubing were used between the surface port and the transducer, and consequently pneumatic lag was less than 0.02 sec. This situation was not a problem for these tests because of the quasi-steady-state nature of the flight test maneuvers. Pressure data were measured and also recorded at 52 Hz.

Hot-Film Sensors

The micro-thin hot-film sensor used in these tests consisted of an array of 45-nickel elements (1 mm long, 0.12 mm wide, and 0.25 μm thick) on a polyimide substrate. The sensor elements were attached to 13 μm

Copyright © 1998, by the International Council of the Aeronautical Sciences (ICAS)
and the American Institute of Aeronautics and Astronautics, Inc.

thick, copper-coated nickel leads that were routed, as shown in Fig. 3, to the airfoil lower surface. The hot-film sensor spacing was designed to be identical with the spacing of the pressure ports. The sensor leads were soldered onto 33-gauge wires that were routed through a narrow slot on the lower surface into the airfoil. Coaxial cables connected these wires to a bank of CVAs inside the FTF. The 'cold' resistance of the sensor elements was 10Ω on the ground and dropped to approximately 8.5 Ω at the flight test altitude, where the ambient temperature was approximately 11° F.

Constant Voltage Anemometer System

The CVA has been described in a number of recent publications[e.g., 20-23]. As the name implies, the sensor is maintained at a constant voltage as shown in the basic circuit (Fig. 4). The voltage level maintained across the sensor determines the current through the sensor and is used for ohmic heating of the sensor. The thermal gradient between the heated sensor and the fluid medium results in heat transfer by convection. The changes in sensor temperature due to this heat transfer results in changes in sensor resistance and the corresponding changes in sensor current is measured across a large resistor R_2.

The output voltage from the CVA is a measure of the convective heat transfer from the surface hot-films. Hence the output voltage is small in laminar boundary layers and high in turbulent boundary layers. The output voltage will also be small when the convective heat transfer and the corresponding shear stress is small as in flow bifurcation regions (leading-edge stagnation point, flow separation and flow reversal regions). In order to effectively detect these critical flow features. the CVA system is equipped with an auto-zero unit which creates a level initial (reference) voltage for all the sensors. The CVA system also incorporates features to automatically set identical desired initial current through all the sensors. Subsequently, the output voltage at any test condition is an indication of relative changes in heat transfer from the reference condition. The CVA instrumentation system, since it operates on a constant voltage basis, does not suffer from the adverse impact of EMI and RFI, cable length (capacitance) does not pose any operational problems (such as instability or oscillations), has high sensitivity and large bandwidth.

Test Approach

Flight data were obtained at an altitude of approximately 20,000 ft during stabilized flight, angle-of-attack sweeps, and acceleration and deceleration maneuvers. Before collecting data, the pilot reset the current in the hot-film and auto-zeroed the circuit output voltage at the test altitude. These objectives were accomplished with a simple push-button remote control switch connected to the instrumentation system. The auto-zeroing was done just once in every flight at a low Mach number (typically 0.50). The stabilized flight points consisted of approximately 20 sec of constant altitude and Mach flight. The angle-of-attack sweeps were typically ±2° in amplitude and were performed at Mach numbers between 0.68 and 0.80. Acceleration and deceleration maneuvers were performed at constant altitude.

The data were telemetered to the ground station and recorded at 1667 Hz. A 3-pole Butterworth filter, having a low-pass roll-off frequency of 503 Hz, was used to pre-sample filter the output voltages measured from the multiple hot-film sensors. For each flight test only 16 of the hot-films were operational. The anemometry system was configured on the ground with the desired set of 16 hot-film sensors for each flight test.

Results and Discussion

The flight Reynolds number range based on airfoil chord for the stabilized flight conditions was between 1.8 and 2.5 million. The boundary layer upstream of the shock at these flight conditions was laminar. Grains of 0.02 in. maximum diameter grit were used in one flight at Mach 0.70 to trip the flow. The presence of the grit made a significant effect on both the pressure and hot-film measurements. As representative cases, the pressure distribution and hot-film voltage outputs are plotted in Fig. 5 for data at Mach 0.70, for laminar (Fig. 5a), and tripped (Fig. 5b) boundary layers. For comparison, the chordwise distribution of signal RMS voltages for the laminar and tripped boundary layer cases are shown in Fig. 6 which clearly shows the large effect of the trip.

A difference in pressure between the two rows of orifices can be seen from the pressure measurements. The difference is largest in the region near the large pressure rise associated with the transonic shock. The differences were observed at each tested Mach number and were caused by a 3D flow on the test article. Note that the boundary layer from the FTF at the test article is approximately 1.5 in. thick[19]. The critical pressure

Copyright © 1998, by the International Council of the Aeronautical Sciences (ICAS)
and the American Institute of Aeronautics and Astronautics, Inc.

coefficient C_p^*, also shown in Fig. 5, is defined as the pressure coefficient corresponding to sonic velocity[24].

Consistent with others in the literature, the shock location is inferred from the pressure measurements to be where the shock-induced rapid pressure rise begins. For the laminar boundary layer case (Fig. 5a), the rapid pressure rise begins approximately at x/c = 0.325 (near hot-film sensor 23), whereas for the tripped boundary-layer case shown in Fig. 5b the rapid pressure rise begins at approximately x/c = 0.275 (sensor 21). Figures 5a and 5b also show mean voltage outputs of hot-film sensors obtained by averaging 1 second of stabilized flight data.

Physical Significance of CVA Output Voltages at Shock Location

The voltage output from the hot-film sensor operated by CVA is a direct indication of the heat transfer from the sensor to the fluid or vice-versa. In subsonic flows, the least heat transfer by convection occurs in the neighborhood of the various flow bifurcation regions such as the leading-edge stagnation, flow separation and flow reattachment regions. At these critical locations the hot-film sensor is a local 'hot spot' since relatively less heat is transferred by convection to the fluid from this sensor. Hence the sensors located at the 'hot spots' have a relatively higher resistance compared to the neighboring sensors and this condition translates to a minimum current through this sensor for a given constant voltage across the sensor. Thus the output from the 'hot spot' sensor will be a minimum. In the presence of shock, the sensor actually gets heated beyond the initial setting and hence the output voltage drops below the auto-zero reference level.

The voltage trends from each sensor during a flight maneuver also convey significant information on the flow characteristics. It is well known that the heat transfer rate and surface shear stress decrease towards the bifurcation region and increase away from it. Thus, during a flight maneuver, as the 'hot-spot' (e.g., shock) approaches a sensor, the output voltage from that sensor decreases due to a decrease in heat transfer. Similarly, as the 'hot spot' moves away from a sensor, its output voltage tends to increase because of an increase in heat transfer. Thus, if two adjacent sensors show opposing output-voltage trends, then it is clear that a 'hot spot' is situated somewhere in between them during that period. We shall use these observations in the following interpretation of the flight test data.

Flight Test Data Analysis

For the laminar boundary-layer case shown in Fig. 5a, the minimum output voltage occurs at x/c = 0.275 (hot-film sensor hf21) which is upstream of the rapid pressure rise (x/c = 0.325) and aft of the minimum pressure location (x/c = 0.25). For the tripped boundary-layer case shown in Fig. 5b, the minimum voltage output occurs at x/c = 0.275 (hf23) which is aft of the rapid pressure rise. Analysis of pressure and hot-film measurements at other Mach numbers showed similar trends. Locations of minimum mean voltages from hot-film sensors for the laminar boundary layer cases are correlated as a function of Mach number in Fig. 7. At all Mach numbers, the location of the minimum mean-voltage hot-film sensor is slightly forward of the pressure inferred shock location.

Although stabilized flights were carried out only at Mach 0.70 for the tripped boundary layer case, data were obtained during a level acceleration maneuver. The acceleration was approximately 3 kn/sec. Figure 8 shows the Mach number at which these hot-film sensors produced the minimum value of output during acceleration. Figure 8 also shows the pressure-inferred shock location. At all Mach numbers, the hot film with minimum output voltage occurs aft of the pressure inferred shock location. This trend was also seen during a level deceleration maneuver.

Angle-of-attack sweeps were made to demonstrate the ability to track the shock location during a dynamic maneuver. Sweeps of approximately ±2° were made at various Mach numbers. Figure 9 shows a time-history of a quasi-steady-state test point followed by an angle-of-attack sweep around Mach 0.70. For this case a laminar boundary layer was present upstream of the shock.

During the first 20 seconds of the maneuver, the angle-of-attack is held constant while the Mach number changes slightly. The angle-of-attack sweep is shown in the last 20 seconds. For simplicity, only four hot-film outputs in the neighborhood of the shock are shown.

For the most part, the sensor hf22 has the minimum output for the first 20 sec of the maneuver. As the angle-of-attack decreased, the shock location shifted to hf23 (20 sec < t < 25 sec) and as the aircraft pulled up the shock location returns to hf22, followed by hf21 and reaches the sensor hf20 at the highest angle-of-attack. Pushing over to trim angle of attack, the shock location reverts to hf22, passing through the other sensors in the reverse order. The movement of the minimum voltage output is consistent with the movement of the shock shown in Fig.

Copyright © 1998, by the International Council of the Aeronautical Sciences (ICAS)
and the American Institute of Aeronautics and Astronautics, Inc.

10 which clearly shows the pressure rise moving aft during the push over, moving forward during the pull up, and then returning to the original position.

Phase Reversal Signatures and Double Frequency

The hot-film outputs are highly sensitive to Mach number variations during the first 20 seconds of the time history (Fig. 9). Hot-films 20 and 21 are in phase with Mach number (i.e., decreasing in output as Mach number decreases and increasing in output as Mach number increases). Hot films 22 and 23 show just the opposite response and are approximately 180° out of phase with Mach number and are therefore out of phase also with hot films 20 and 21. The phase reversal between hot films 21 and 22 can also be an indicator of the shock location[20]. Phase reversal about the hot film with the minimum output was observed at all Mach numbers tested.

Let us consider the trends in sensor output voltages a little more closely. The time trace hf22 increases initially from t = 0 to t = 10 sec and at the same time the output from the neighboring sensor hf21 decreases. As described earlier, this situation shows that the 'hot spot' (shock) is moving away from hf22 and moves towards hf21. Actually they cross each other for a short time around t = 10 sec indicating that the shock location was at or closer to the sensor hf21 for the given flight conditions at t = 10 sec. The respective sensor output voltages again diverge beyond this time, with hf21 increasing in magnitude while hf22 decreases, indicating that the shock has moved farther away from hot-film sensor 21 location. The hot-film sensor hf22 with minimum output voltage is still located closest to the shock. At about t = 20 sec, hf22 reaches its minimum and begins to increase. We can conclude that at this flight condition the shock was located exactly at the hot-film sensor 22. As the angle-of-attack is further reduced we observe that output voltage from hf23 starts decreasing rapidly and crosses hf22 at about t = 22 sec and beyond this point the shock is located closer to hf23. In the meanwhile hf21 has continued to increase rapidly and even goes positive showing that it has entered a more highly convective region and relatively cooled by the boundary-layer flow. The sensor hf23 reaches its own minimum at approximately t = 24 sec indicating that the shock was located at hf23 at the given flight conditions (low alpha, high Mach number). Every cross-over point indicates that the shock is moving away from sensor with increasing voltage and moving towards the sensor with decreasing voltage, and at the cross-over point the shock is located between them. The rest of the figure can be similarly explained.

It is interesting to see that hf20 which practically remained dormant for the most part of this flight dramatically dropped in voltage around t = 30 sec, when the aircraft angle-of-attack reached its maximum value and the Mach number approached its minimum. Also, for the entire duration of this maneuver hot films 21 and 23 were basically out of phase with each other indicating that the shock was located between them during the entire period. Another interesting feature of the test results is that for 15 sec.<t<35 sec. the signal from hf22 exhibits a frequency that is approximately twice that of the other hot films during the angle-of-attack sweep indicating that the shock oscillates around this sensor during this maneuver. Similar double frequency is observed in hf21 near the highest angle-of-attack conditions (t ≈ 30 sec). Another important observation that is consistent with earlier studies is the relative low amplitude fluctuation of signals from the sensor located at the mean-shock position. For example, for 27 sec.<t<35 sec., when the angle-of-attack reaches its maximum and starts to decrease the mean shock position oscillates about the sensor hf21. We can observe that the amplitude of fluctuation for hf21 is significantly lower and exhibits double-frequency oscillations compared to neighboring sensors for the given period. Similarly, for the entire alpha sweep, the sensor hf22 where the mean shock was located exhibits a low-amplitude, double-frequency characteristic.

As the angle-of-attack and the Mach number returned to their trim values (t > 35 sec), the sensor outputs also returned to their initial values showing that the approach used in these flight tests was very effective and repeatable.

Flow Structure Near the Shock

These flight test results show that both minimum mean voltage and phase reversal signatures are potential indicators of the shock location. At some transonic Mach numbers, two distinct minimums occur in the hot-film outputs as seen in Fig. 5. This second minimum is suspected to be associated with the second leg of a lambda shock. In terms of the surface characteristics, the front leg of the lambda shock is associated with flow separation while reattachment occurs near the rear leg (Fig. 1).

There are two concurrent effects present in the shock region: (1) the sensor is heated by the presence of the shock and (2) heat is transferred from the sensor by convection. Less heat is taken away from the sensor, which is located at a flow bifurcation region such as flow separation and flow reattachment where the convective

Copyright © 1998, by the International Council of the Aeronautical Sciences (ICAS)
and the American Institute of Aeronautics and Astronautics, Inc.

heat transfer is a minimum. Hence, we are observing the combined effect of these two independent phenomena. The presence of a negative voltage indicates that the heating due to the shock is greater than heat transfer by convection and the minimum voltage indicates the presence of a flow bifurcation point. The phase reversal signature, double frequency, and low amplitude signals from the sensor at the mean shock location indicate that the flow oscillates about the bifurcation point.

A comparison of hot-film output minimums with the pressure distributions in Fig. 5 indicates that the separation region began farther upstream of the shock when the flow was laminar than when it was tripped. It also indicates that the forward leg of the lambda shock was situated farther ahead of the main shock in the laminar case. This result is consistent with the fact that turbulent boundary layers can withstand larger pressure gradients before separation. Another observation from Fig. 5 is that the hypothesized separation and reattachment points are farther apart for the laminar boundary layer case. The separation and reattachment points are 12.5% chord apart for the laminar boundary layer case and only 7.5% of the chord for the tripped flow case.

Further evidence of the shock-induced separation bubble can be seen in the power spectral densities (PSD) of the hot films (Fig. 11) for data obtained at Mach 0.70. For this flight condition, the hot-film minimums (Fig. 5a) were at hf21 and hf26 indicating a bubble between them. The PSD analysis of nose boom angle-of-attack signal showed a peak near 13 Hz at this Mach number because of an unknown origin. Figure 11 shows PSD of hf19, hf25, and hf27. The 13Hz signal is present in hf19 and hf27 which are located outside the bubble and not in hf25 which is inside the bubble. It is presumed that the shock-induced separation phenomenon did not allow the external signal source at 13 Hz to penetrate the bubble. Tests at other Mach numbers also showed that this observation was typical of PSD magnitudes from hot films between two minimums. Such observations suggest that this phenomenon could also be used to define the extent of the lambda shock. as well as the extent of the separation bubble.

Conclusion

Successful flight tests were conducted on F-15B aircraft at NASA Dryden Flight Research Center to detect transonic shock in stabilized and quasi-steady flight conditions. Results show that simultaneous boundary-layer measurements using an array of surface hot-film sensors, multi-channel CVA instrumentation system, and advanced flow diagnostics techniques provide a viable approach for in-flight detection and characterization of transonic shock dynamics.

Acknowledgment

Tao Systems is thankful to NASA Dryden Flight Research Center and its F-15 flight-test crew for supporting the flight experiment. Authors are also thankful to T.S. Kwa, Bob Lankes and Bob Pfouts of Tao Systems for their assistance with instrumentation and data analysis.

References

1. Loving, D.L., *"Wind Tunnel -- Flight Correlation of Shock-Induced Separated Flow"*, NASA TN D-3580, Sept. 1966.
2. Pearcey, H.H. and Holder, D.W., *"Examples of the Effects of Shock-Induced Boundary-Layer Separation in Transonic Flight"*, Ministry of Technology, Aeronautical Research Council, R&M No. 3510, Jan. 1954.
3. Seddon, J. and Goldsmith, E.L., *"Intake Aerodynamics"*, AIAA Education Series, AIAA and BSP Professional Books, 1985.
4. *"Shock-Wave Boundary Layer Interactions"*, AGARDograph No. 280, Feb. 1986.
5. *"Transonic Aerodynamics"*, AGARDograph No.35, Sept. 1968.
6. Mangalam, S.M., Stack, J.P. and Sewall, W.G., *"Simultaneous Detection of Separation and Transition in Surface Shear Layers. Fluid Dynamics of Three-Dimensional Turbulent Shear Flows"*, AGARD CP-438, 1988.
7. Mangalam, S.M., Sarma, G.R. and Kuppa, S., *"Quantitative Flow Diagnostics Techniques for Unsteady Aerodynamics"*, PICAST2-AAC6 International Conference, Australia, 1995.
8. Mangalam, S.M. and Suryanarayan, S., *"Critical Aerodynamic Flow Feature Indicators (CAFFI) as Higher Level Control Inputs for Future Aircraft"*, ICAS 94, Sept., 1994.
9. Mangalam, S.M., *"Instrumentation System for Determining Flow Stagnation Points"*, U.S. Patent No. 5,218,863., June 1993.
10. Ludwig, H., *"Instrument for Measuring the Wall Shearing Stress of Turbulent Boundary Layers"*, NACA TM-1284, 1950.
11. Liepmann, H.W. and Skinner, G.T., *"Shearing Stress Measurements by Use of a Heated Element"*, NACA TN-3268, 1964.

Copyright © 1998, by the International Council of the Aeronautical Sciences (ICAS)
and the American Institute of Aeronautics and Astronautics, Inc.

12. Houdeville, R. and Juillen J.C., *"Skin Friction Measurement With Hot Elements"*, in VKI Lecture Series 1989-05, Measurement Techniques in Aerodynamics, April 1989.
13. Bellhouse, B.J. and Schultz, D.L., *"Measurement of Skin Friction in Supersonic Flow by Means of Heated Thin Film Gages"*, Aeronautical Research Council R&M 3490, London, Oct. 1965.
14. Hartidonis, J.H., *"The Measurement of Wall Shear Stress"*, Adv. in Fluid Mechanics Measurements, Springer-Verlag, Berlin, 1989.
15. Owen, F.K., *"Transition Experiments on a Flat Plate at Subsonic and Supersonic Speeds"*, AIAA Journal, vol. 8, 1970.
16. Rubesin, M.W., Okuno, A.T., Mateer, G.G. and Brosh, A.A., *"A Hot-Wire Surface Gage for Skin Friction Measurements and Separation Detection"*, NASA TM X-62465, 1975.
17. Abbott, I.H. and Von Doenhoff, A.E., *"Theory of Wing Section"*, Dover Publications, Inc., 1959.
18. Moes, T.R., Sarma, G.R., and Mangalam, S.M., *"Flight Demonstration of a Shock Location Sensor Using Constant Voltage Hot-Film Anemometry"*, NASA TM 4806, Aug. 1997 (Also presented at SFTE Conference, Orlando, FL, Aug. 1997.
19. Richwine, D.M., *"F-15B/Flight Test Fixture II: A Test Bed for Flight Research"*, NASA TM-4782, Dec. 1996.
20. Sarma, G.R., *"Analysis of a Constant Voltage Anemometer Circuit"*, IEEE/IMTC Conference, May 1993.
21. Comte-Bellot, G., *"Hot-Wire Anemometry"*, Handbook of Fluid Dynamics, ed. R.W. Johnson, CRC Press, 1998.
22. Kegerise, M.S. and Spina, E.F., *"A Comparative Study of Constant Voltage and Constant Temperature Hot-Wire Anemometer in Supersonic Flows"*, 3rd International Symposium on Thermal Anemometry, San Diego, CA, July 1996.
23. Sarma, G.R., *"Transfer Function Analysis of the Constant Voltage Anemometer"*, Review of Scientific Instruments, to be published June, 1998.
24. Shapiro, A.H., *"The Dynamics and Thermodynamics of Compressible Fluid Flow"*, The Roland Press Company, New York, 1954.

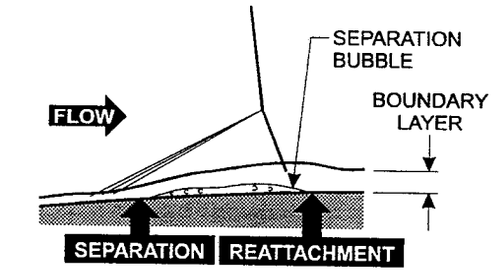

Figure 1. Hypothesized flow structure near the shock.

Fig. 2. The F-15B in flight with the FTF and test article installed.

Copyright © 1998, by the International Council of the Aeronautical Sciences (ICAS)
and the American Institute of Aeronautics and Astronautics, Inc.

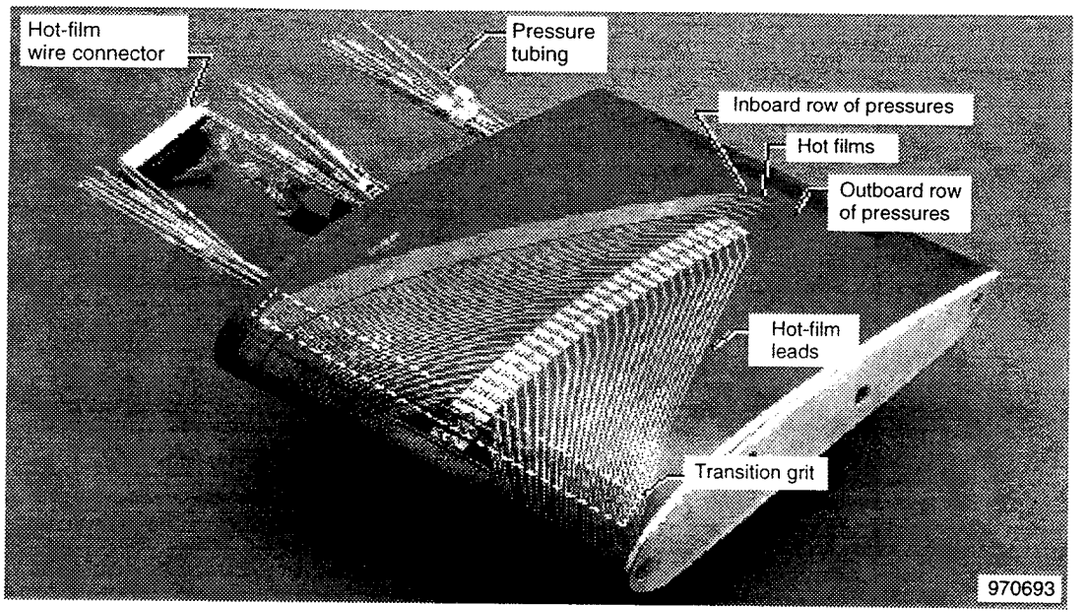

Fig. 3. The test article showing upper surface instrumentation and the grit strip

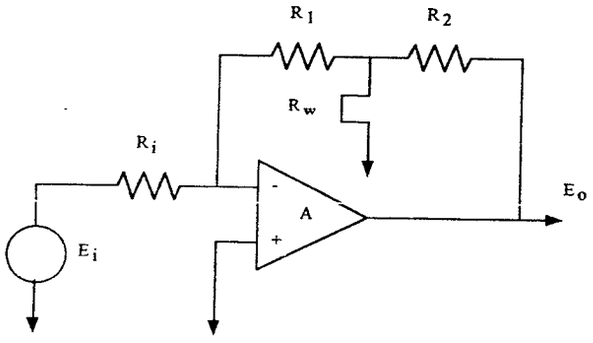

Fig. 4 Basic Constant Voltage Circuit

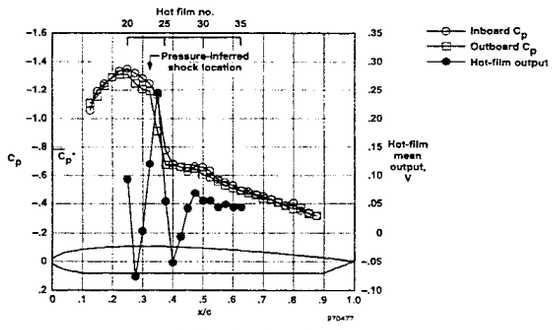

(a) Laminar boundary layer.

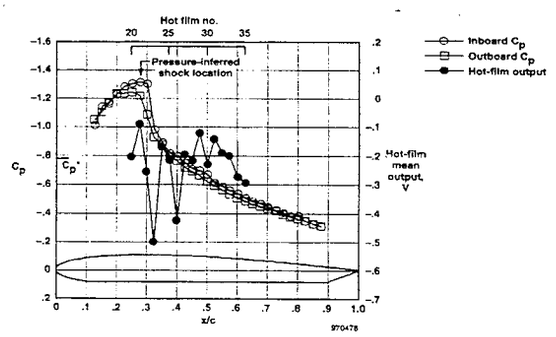

(b) Tripped boundary layer.

Fig. 5. Pressure and hot-film mean voltage distributions for stabilized flight at Mach 0.7

Copyright © 1998, by the International Council of the Aeronautical Sciences (ICAS)
and the American Institute of Aeronautics and Astronautics, Inc.

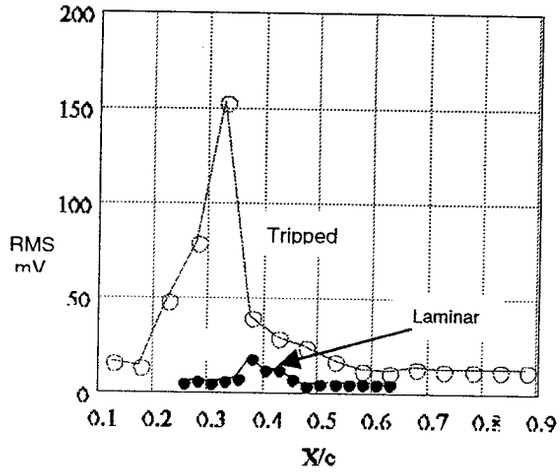

Fig. 6. RMS distribution for laminar and tripped boundary layers

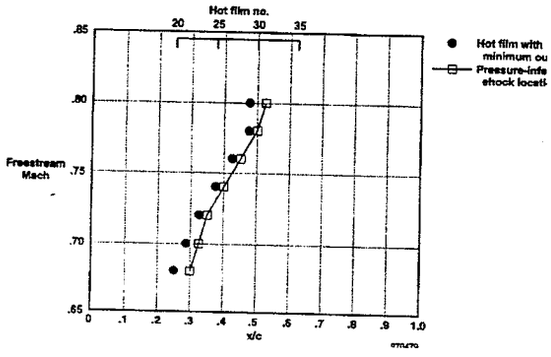

Fig. 7. Comparision of hot-film minimum voltages with pressure-inferred shock locations for a laminar boundary layer

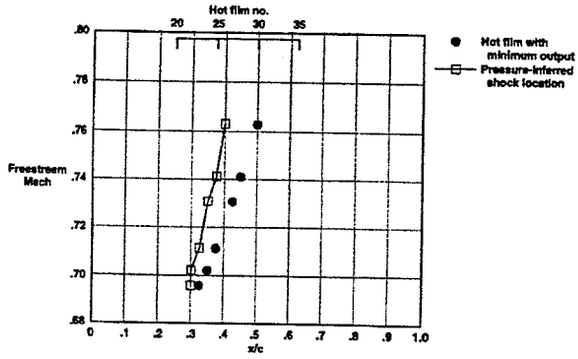

Fig. 8. Comparison of hot-film minimum voltage with pressure-inferred shock locations for a tripped boundary layer.

Copyright © 1998, by the International Council of the Aeronautical Sciences (ICAS)
and the American Institute of Aeronautics and Astronautics, Inc.

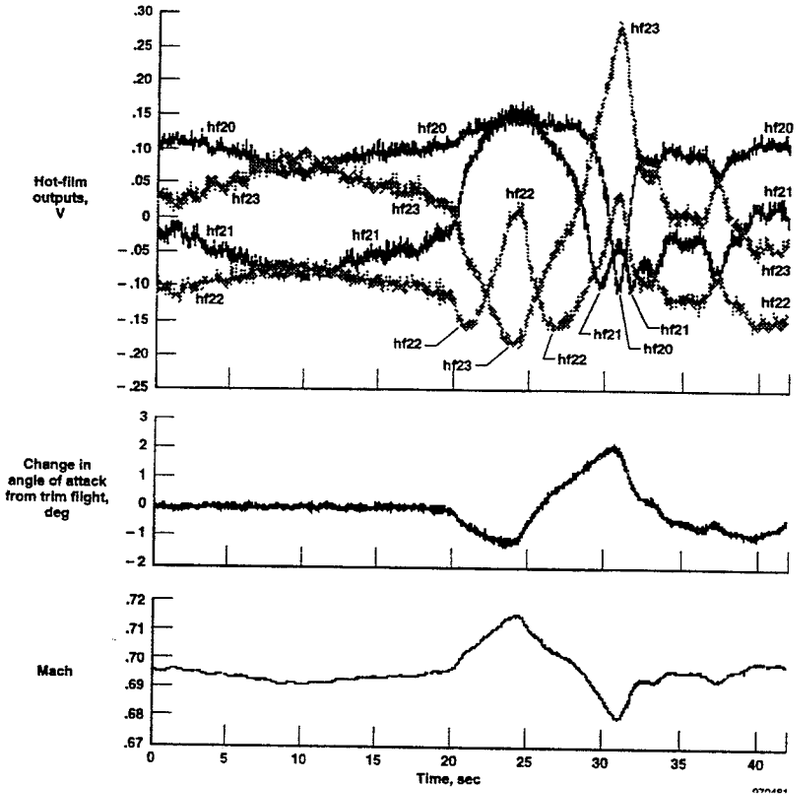

Fig. 9. Time history of stabilized flight and angle-of-attack sweep at Mach 0.7.

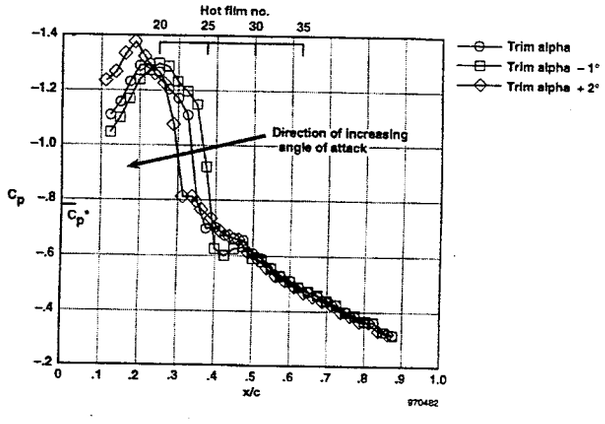

Fig.10. Pressure distribution during an angle-of-attack sweep at Mach 0.7

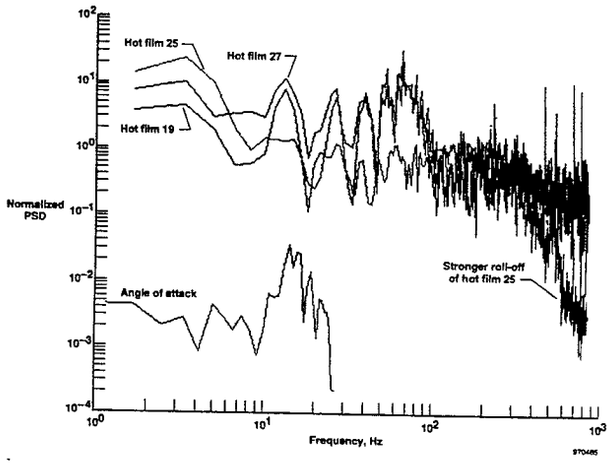

Fig.11. Power spectral densities of hot films 19, 25, and 27 and angle-of-attack during a stabilized test point at Mach 0.7